

PCCP

Accepted Manuscript



This is an *Accepted Manuscript*, which has been through the Royal Society of Chemistry peer review process and has been accepted for publication.

Accepted Manuscripts are published online shortly after acceptance, before technical editing, formatting and proof reading. Using this free service, authors can make their results available to the community, in citable form, before we publish the edited article. We will replace this *Accepted Manuscript* with the edited and formatted *Advance Article* as soon as it is available.

You can find more information about *Accepted Manuscripts* in the [Information for Authors](#).

Please note that technical editing may introduce minor changes to the text and/or graphics, which may alter content. The journal's standard [Terms & Conditions](#) and the [Ethical guidelines](#) still apply. In no event shall the Royal Society of Chemistry be held responsible for any errors or omissions in this *Accepted Manuscript* or any consequences arising from the use of any information it contains.

Effect of Sulfate Pre-treatment to improve deposition of Au-nanoparticles in Gold-Modified sulphated g-C₃N₄ plasmonic photocatalyst towards visible light induced water reduction reaction

Sulagna patnaik¹, Satyabadi Martha¹, Giridhar Madras² and Kulamani Parida^{1*}

¹Centre for Nano Science and Nano Technology, SOA University, Bhubaneswar-751030

²Department of Chemical Engineering, Indian Institute of Science, Bangalore

Abstract

In continuation of our earlier work on Au-g-C₃N₄ and to improve the activity further, Au incorporated sulfated carbon nitride (g-C₃N₄) has been designed by using a simple impregnation cum borohydrate reduction method for visible light induced water reduction reaction for hydrogen generation. The photocatalysts were characterized by various instrumental methods such as PXRD, UV-Vis DRS, SEM, HR-TEM, XPS, PL and TRPL spectral analysis. The functionalisation by -HSO₃ group and incorporation of AuNPs in g-C₃N₄ skeleton extends its pi-conjugated system, modifies its semiconductor properties, such as the band structure engineering with tunable bandgap, red-shift of the optical absorption and promoting the charge migration and separation. Sulfate pre-treated g-C₃N₄ samples were supposed to have a defected surface due to oxygen vacancy, which strengths the adsorption of AuNPs onto the vacant oxygen sites. Thus the AuNPs get adsorbed on the reduced surfaces, increasing the extent and effectiveness of the electronic communication between gold and the g-C₃N₄ interface. The improved photocatalytic activity could be attributed to the surface plasmon resonance (SPR) effect of AuNPs which synergistically facilitates the photocatalysis process. The photocatalytic activity of Au-sulfated g-C₃N₄ for photocatalytic splitting of water to produce H₂ was increased 1.5 times than Au-g-C₃N₄, 2.5 times than sulphated-g-C₃N₄ and 35 times than that of single-phase g-C₃N₄.

*Corresponding author

E-mail: kulamaniparida@soauniversity.ac.in, paridakulamani@yahoo.com,
martha.satyabadi@gmail.com

Tel. No. +91-674-2351777

Fax. +91-674-2350642

Introduction

To satisfy increasing global energy demands and to resolve the environmental problems, it is highly essential to develop methods for sustainable energy conversion and storage technologies [1]. The conversion of solar light into hydrogen fuel by splitting water is one of the most promising solutions for sustainable energy sources. During the past few decades, many researchers were working for the development of efficient, sustainable, visible-light-induced semiconductor photocatalysts to directly convert solar energy into chemical energy and produce hydrogen fuel by splitting water [2]. A variety of photocatalytic nano-structured materials have been developed for solar energy conversion due to their unique properties like appropriate band gap to show a strong visible light response, with a high photocatalytic performance, non-toxicity, good thermal and chemical stability. Also these semiconductor photocatalysts must be comprised of earth-abundant elements, synthesised easily with a tailored porosity and must follow a green pathway.

To overcome these difficulties the most emerging nanostructured visible light induced photocatalytic materials is graphitic-carbon nitride ($g\text{-C}_3\text{N}_4$). Nanostructured $g\text{-C}_3\text{N}_4$ is an appealing class of nanomaterial as it is composed of earth's most-abundant elements carbon and nitrogen only and "sustainable". It not only fulfils all the requirements of a good photocatalyst but also can be easily synthesised from simple cost effective nitrogenous starting materials. Polymeric metal free graphitic carbon nitride ($g\text{-C}_3\text{N}_4$) is a layered nanostructured material having alternate Carbon and Nitrogen atoms with a structure similar to that of graphene. It is composed of two-dimensional networks of tri-s-triazine connected through tertiary amines groups which makes it to have high thermal stability (up to 600 °C in air) and chemical stability (towards acids, bases, and different organic solvents) due to the presence of strong covalent bonds between C and N atoms. It is a visible-light-active semiconductor photocatalyst having band gap energy of 2.7 eV, absorbs optical wavelength upto 450 nm, having an appropriate band potential for both water oxidation and reduction [3], for which $g\text{-C}_3\text{N}_4$ promptly becomes a shining star in the field of photocatalysis. It has been extensively reported that $g\text{-C}_3\text{N}_4$ with different structural modifications shows different properties such as chemical inertness, hardness, low friction coefficient, high potential for solar energy conversion, storage and also in environmental remediation such as photocatalysis in fuel cells, catalysis, or CO_2 reduction to reduce the emissions of greenhouse gases [4-6]. Although $g\text{-C}_3\text{N}_4$ has a promising potential in the domain of

photocatalysis, still the photocatalytic efficiency of neat g-C₃N₄ is restricted due to, 1) Low efficiency for electron hole separation, 2) Neat g-C₃N₄ can absorb only blue light of the solar spectrum which restricts the utilization of the whole solar spectrum, 3) The high degree of polycondensation of the monomers during the synthesis renders the materials with low surface area of g-C₃N₄ (~10 m²/g) without forming porous texture and 4) the grain boundary effects which disrupt the delocalization of electrons.

For optimizing the materials, various methods have been proposed to enhance its photocatalytic activity such as by reducing the grain size which is in general a most common solution for improving delocalization of electrons. Therefore, optimising the material by band gap engineering with other modification is introduced for the improvement of the performance of g-C₃N₄. Many efforts have been made to synthesize g-C₃N₄ crystals to extend pi-electron delocalization by preparing nanoporous and mesoporous g-C₃N₄, preparing morphology controlled g-C₃N₄ (nano-rods, spheres, sheets), doping with non-metals like B, S, P, F, I etc. protonating g-C₃N₄ by strong acids, preparing heterojunction/composite with another semiconductor, introducing N-vacancies in the frame work of g-C₃N₄, by incorporating with metals (specially noble metals like Ag, Pt, Au, etc), by exfoliating g-C₃N₄ and also by chemical grafting of surface functional groups [7,8].

It is also well known that, nanoparticles of noble metals such as Ag, Au, Pt can effectively absorb visible light and enhance the efficiency of photocatalytic processes by favouring interfacial charge transfer in semiconductor owing to their surface plasmon resonance (SPR) resulted from the oscillation of surface electrons. The role of Au NPs are found to be superior among all noble metals for visible light induced photocatalytic hydrogen production owing to their surface plasmon effects, low photoluminescence intensity, reduced band gap energy and superior visible light absorption [9].

Various group of researchers extensively studied the effect of acid treatment on g-C₃N₄ and gold modified photocatalysts by varying the wt% of gold. Zhang et al. studied the photocatalytic activity of protonated g-C₃N₄ and found that the improved activity is mostly due to better dispersion, enhanced surface area and surface functionality [10]. Ma et al. reported synthesis of g-C₃N₄ nanosheets with the thickness of 2–4 nm (i.e. 6–12 atomic monolayers) with enhanced fluorescence intensity and excellent water dispersion stability due to their surface protonation [11]. Yan et al. found an increased H₂ evolution by synthesising g-C₃N₄ from sulfonated melamine [12]. Cheng et al. prepared stable ultrathin nanosheets of g-C₃N₄ in large scale by using H₂SO₄ [13]. Chang et al. reported significant role of AuNPs in improving the photocatalytic activity of g-C₃N₄ under UV-radiation [14]. Singh et al. studied

the importance of basic –OH groups in Au nano-particle supported g-C₃N₄ [15]. Cheng group reported the photocatalytic activity of exfoliated g-C₃N₄ nano sheets by loading Au-nanoparticles [16]. The Plasmon enhanced photocatalytic activity of g-C₃N₄ under visible light irradiation has been studied by Xue et al. [17]. Our group also reported the increased hydrogen evolution rate in case of 1 wt% Au-loaded g-C₃N₄ composite plasmonic photocatalyst [9].

In the present study, we have tried to find out the effect of sulfate loading in improving the deposition of Au over g-C₃N₄ and enhancing the activity of Au-g-C₃N₄ nanocomposites. We have tried to modulate the surface functionality and electronic structure of the pi-conjugated polymeric graphitic carbon nitride by increasing its surface functionality by means of sulfonation to form a stable pi-conjugation system. The introduction of surface active groups are supposed to create surface dyadic structures, which accelerates the charge transfer from bulk-to the surface and improves the charge separation. The sulphate pre-treatment samples were found to possess defected surface due to the formation of oxygen vacancies, which strengthens the adsorption of AuNPs onto the vacant oxygen sites. AuNPs preferably get adsorbed on the defected surface, by increasing the extent and effectiveness of the electronic communication between AuNPs and the g-C₃N₄ interface. By considering the importance of sulfonation to deposit Au nanoparticles, we have deposited AuNPs on the sulfated surface of g-C₃N₄ and observed that the photocatalytic performances of g-C₃N₄ are significantly enhanced after incorporating Au NPs.

Experimental section

All the chemicals used for synthesis of Au loaded sulphated g-C₃N₄ plasmonic photocatalyst were analytical grade and were used without further purification. The principal synthesis involves three steps:

Synthesis of neat g-C₃N₄

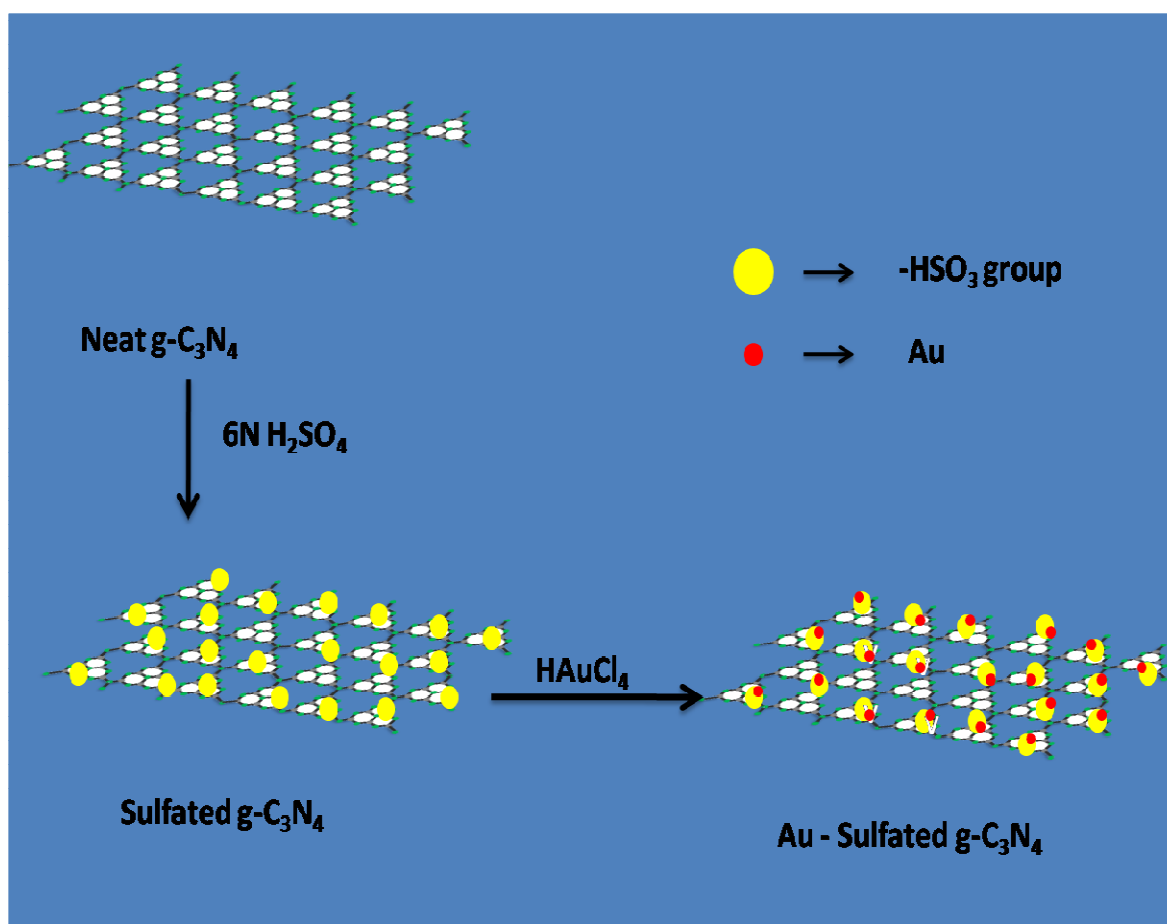
The g-C₃N₄ nano-powder was synthesized by one-step thermal polymerization of melamine in a semi closed system to prevent sublimation. 10 g of melamine was put into an alumina crucible with a lid, and then heated at 550°C for 4h with a heating rate of 4°C per minute in a muffle furnace. After natural cooling to room temperature, the resultant yellow solid was collected and ground into powder for further treatment.

Synthesis of sulfated g-C₃N₄

1g of the prepared g-C₃N₄ powder was dispersed in 10 mL of deionized water and magnetically stirred for 1h. A calculated amount of 6N H₂SO₄ was added and subsequently heated at 60 °C with constant stirring to evaporate until a slurry was formed. The slurry was then dried in an oven at 80 °C for 12 h. The obtained solid was calcined at 400°C for 2 h in a muffle furnace to remove any impurities. By adding different calculated amount of 6N H₂SO₄, 3wt%, 6wt%, 9wt%, 12wt% sulfated g-C₃N₄ were obtained.

Synthesis of Au loaded sulfated g-C₃N₄ plasmonic photocatalyst

Au nanoparticle decorated g-C₃N₄ organic hybrid plasmonic photocatalyst was prepared by a borohydrate-reduction method. 1g of sulfated g-C₃N₄ synthesised by taking melamine was dispersed in 100 mL of deionized water and magnetically stirred for 2h. For 1 wt% Au NPs, 16.5 mL of 0.01 M HAuCl₄ acid was added in a drop wise manner and the solution was aged for 30 minutes. A 15% NH₃ solution was added to maintain the pH at 8-9. Freshly prepared NaBH₄ solution in ice cold water was injected rapidly. Immediately after the addition of NaBH₄ solution, a red colour precipitate of AuNPs was formed. The resultant precipitate was washed several times with 200 mL of DI water each time and dried for 12 h in the oven at 100°C. The greyish-red coloured precipitate was collected and ground into powder for further use. The Au-sulfated g-C₃N₄ (1 wt% Au) were also prepared by following the same procedure for 3wt%, 6wt%, 9wt%, 12wt% sulfated g-C₃N₄ samples for comparison. For comparison study, 1%Au-g-C₃N₄ is prepared by the similar method without sulphate treatment.



Scheme 1 Scheme for the fabrication of Au loading in sulphated g-C₃N₄ nanocomposite.

Analytical characterisation

The crystallinity of as-synthesized photocatalysts were analyzed by Advanced Powder X-ray diffraction (PXRD) on Rigaku Miniflex (set at 30 kV and 15 mA) powder diffractometer using Cu K α radiation ($\lambda = 1.54 \text{ \AA}$). Diffraction patterns were recorded over 2θ angle range ($10^\circ < 2\theta < 60^\circ$) with a scan rate of $2^\circ/\text{min}$. UV-vis diffuse reflectance spectra were conducted to study optical absorbance of all the photocatalysts by UV-vis spectrophotometer (Varian Cary 100) in the region 200-800 nm, with boric acid as a reflectance standard and by converting reflectance to absorbance by the Kubelka-Munk method, The Brunauer-Emmett-Teller (BET) specific surface area of samples was measured by N₂ adsorption-desorption studies using Automated Surface area and Porosity Analyser (ASAP 2020, Micromeritics,

USA) at liquid nitrogen temperature ($-197\text{ }^{\circ}\text{C}$). Before analysis, the samples were degassed under vacuum (10^{-5} torr) at $300\text{ }^{\circ}\text{C}$ for 4 h. Fourier transform infrared (FT-IR) spectra of the samples was performed on Bruker ALPHA FT-IR spectrometer at the frequency range of $4000\text{--}500\text{ cm}^{-1}$ with a resolution of 4 cm^{-1} with KBr as the reference diluents. X-ray photoelectron spectroscopy (XPS) measurements were carried out by using a non-monochromatised Mg-K α X-ray source on a VG Microtech Multilab ESCA 3000 spectrometer. Energy resolution of the spectrometer was set at 0.8 eV with Mg-K α radiation at pass energy of 50 eV . The elementary composition and bonding information of samples were obtained by measuring the binding energies taking the C 1s peak of carbon at 284.9 eV as a reference. The surface morphology and the chemical composition of as-prepared samples were measured by TEM and HRTEM images on Philips TECNAI G² instrument at an accelerating voltage of 200 kV . SEM images were analysed by a Hitachi S-3400N. Prior to the analyses, the samples were sputtered with a thin film of gold. The powder particles were supported on a carbon film coated on a 3 mm diameter fine-mesh copper grid. A suspension in ethanol was sonicated and a drop was dripped on the support film. PL spectrum was recorded with a LS 55 fluorescence spectrophotometer at room temperature and the excitation wavelength was 350 nm .

Results and discussion

XRD analysis

The crystal phase, interlayer stacking, crystallite size and structure of the prepared composite were determined by PXRD analysis. Two distinct diffraction peaks are obtained for neat g-C₃N₄. A stronger diffraction peak at 27.4° indexed as 002 plane which represents graphitic like layered stacking with interlayer distance of 0.326 nm and a minor peak at 13.1° corresponds to 100 plane with inter planar separation of 0.68 nm [18].

It is found from figure 1(a) that even after sulphonation and Au-loading the same diffraction patterns are maintained in g-C₃N₄, which indicates that the aromatic motif of tri-s-triazine is chemically robust towards any structural modification. Highly intense peak at 27.4° indicates higher crystallinity of g-C₃N₄ with the existence of fewer bulk defects. With increase in the extent of sulfonation, the intensity of 002 peaks remarkably decreases and the peak broadens showing strong interaction between $-\text{HSO}_3$ group and g-C₃N₄. Increase in SO_4^{2-} content also inhibits the growth of g-C₃N₄ layer. It also signifies the size of g-C₃N₄ decreases, which has

positive effect towards photo-catalytic application. With Sufonation, the 002 peak is slightly shifted to higher 2θ value indicating decrease in gallery distance and a denser stacking. In figure 1A the diffraction peaks at $2\theta = 38^\circ$, 44° and 78° in sample a, c, and d are mostly due to the presence of impurities. From figure 1 (b), it is observed that after incorporation of Au NPs on neat g-C₃N₄ and sulphated g-C₃N₄, four separate reflections at 38.23° , 44.24° , 64.73° and 78.8° are revealed corresponding to (111), (200), (220) and (311) plane respectively along with the planes of g-C₃N₄ [9]. From the XRD pattern of 1%Au-g-C₃N₄, it is found that the crystallinity of Au nanoparticles is less as compared to that of 1% Au sulphated g-C₃N₄. Moreover, it is observed that the peak intensity of Au nanoparticles increases with the increase in wt% of sulfate, indicating the rise of long- range order and crystallinity in the sample. Among the three reflections due to Au NPs, the most intense 38.23° peak indicates (111) plane is the predominating crystal plane in the composite. It is also observed that wt percentage of sulfate enhances the crystallinity of Au, which acts as co-catalyst to enhance the photo-catalytic activity. It is revealed that there exists an electrostatic interaction between SO_4^{2-} and Au nanoparticles. 9 wt% sulfated g-C₃N₄ with 1 wt% Au loading increases the activity due to synergistic effect between SO_4^{2-} and Au nanoparticles. But higher wt% of sulfate results agglomeration on the surface of g-C₃N₄ which hinders the growth of (111) plane of Au.

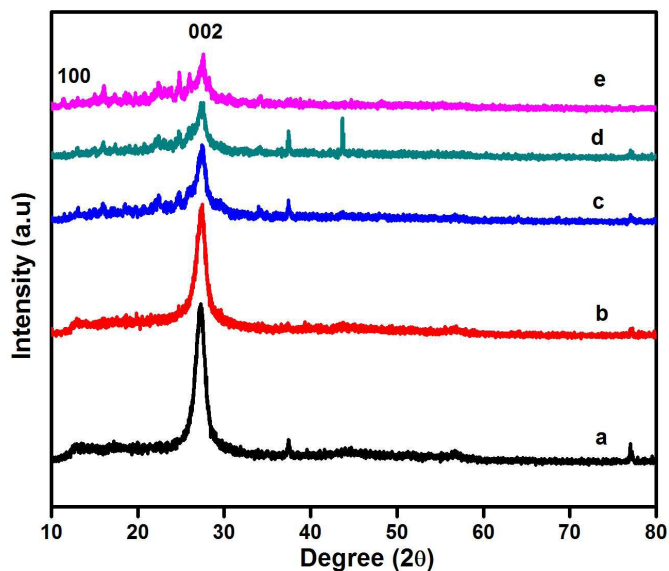


Figure 1 (a) PXRD patterns of (a) neat g-C₃N₄ (b) 3% SO₄ g-C₃N₄ (c) 6% SO₄ g-C₃N₄ (d) 9% SO₄ g-C₃N₄ and (e) 12% SO₄ g-C₃N₄

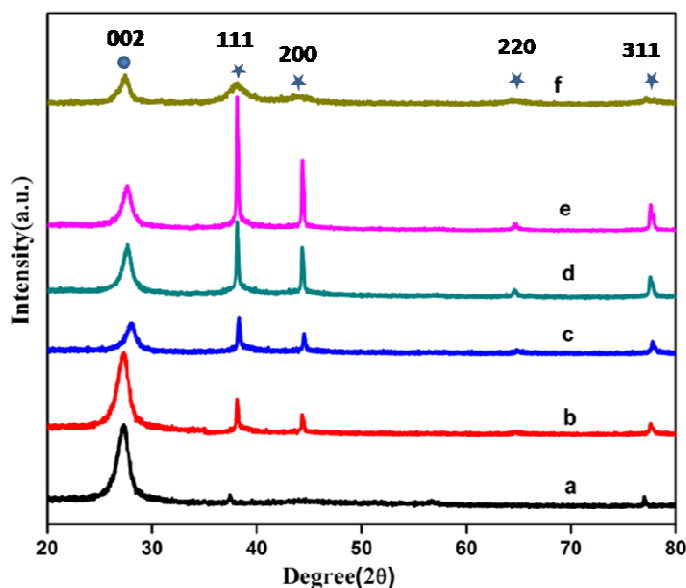


Figure 1 (b) PXRD patterns of (a) neat $g\text{-C}_3\text{N}_4$ (b) 1%Au- $g\text{-C}_3\text{N}_4$ (c) 1%Au-3% SO_4 $g\text{-C}_3\text{N}_4$ (d) 1%Au-6% SO_4 $g\text{-C}_3\text{N}_4$ (e) 1%Au-9% SO_4 $g\text{-C}_3\text{N}_4$ and (f) 1%Au-12% SO_4 $g\text{-C}_3\text{N}_4$

FTIR spectroscopy

The FTIR spectra of neat $g\text{-C}_3\text{N}_4$ and all Au loaded sulfated- $g\text{-C}_3\text{N}_4$ samples are shown in Figure 2. The FTIR data of all Au loaded sulfated $g\text{-C}_3\text{N}_4$ samples are in consistent with the previous reported results [9]. A broad absorption band near the high-frequency region at approximately $3000\text{--}3500\text{ cm}^{-1}$ is mainly attributed to symmetric and anti-symmetric stretching vibrational modes of NH and NH_2 associated with uncondensed NH_2 groups and absorbed H_2O molecules. The vibrational bands at $1000\text{--}1700\text{ cm}^{-1}$ and 832 cm^{-1} in the FTIR spectra represents the characteristics of C=N and C-N stretching vibrations of CN heterocycles and triazine ring modes, respectively, all consistent with that of coplanar nature

of g-C₃N₄. Generally, the vibrational band due to Au-O was observed at 818 cm⁻¹. No other vibrational band was observed for the Au-O in the FTIR spectra because of the overlapping between the vibrational peak of Au-O with the out of plane bending vibrational modes of CN heterocycles [9]. For Au loaded sulfated g-C₃N₄ composites, all the characteristic vibrational peaks of g-C₃N₄ are retained, suggesting that the crystal structure of g-C₃N₄ was not changed after modification by Au nanoparticles.

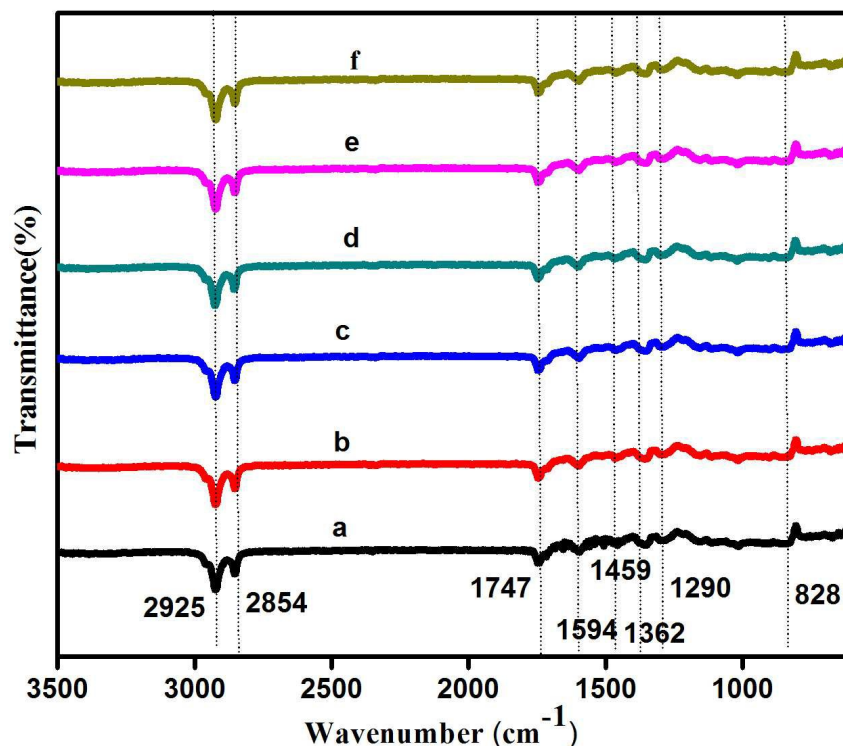


Figure 2 FTIR Spectra of (a) neat g-C₃N₄ (b) 3% SO₄ g-C₃N₄ (c) 6% SO₄ g-C₃N₄ (d) 9% SO₄ g-C₃N₄ (e) 12% SO₄ g-C₃N₄ and (f) 1% Au-9% SO₄ g-C₃N₄

Scanning electron microscopy (SEM)

The surface topography and the elemental composition of the prepared samples were investigated by SEM. From the SEM images, it can be revealed that a typical slate-like, stacked lamellar structure was formed in case of neat g-C₃N₄. Many mesopores are found to present in those lamellar structures, which is due to the release of a large number of gases such as NH₃ and CO₂ during the thermal condensation of melamine [19]. However, after sulfonation, the g-C₃N₄ network may decompose to form clusters of condensed triazine-rings,

yielding irregular porous network and thin lamellar structures and the specific surface area is therefore enlarged. Moreover, this porous structure may also provide more active sites for reactants, by increasing the defects on the surface of $g\text{-C}_3\text{N}_4$, thereby providing growth sites for AuNPs and promote photocatalytic reactions. After incorporation of 1wt% AuNPs on the $g\text{-C}_3\text{N}_4$ network as shown in figure 3 many nano-crystals of gold get uniformly dispersed on the surface of sulfated $g\text{-C}_3\text{N}_4$. The elemental composition of neat $g\text{-C}_3\text{N}_4$, sulfated $g\text{-C}_3\text{N}_4$ and Au loaded sulfated $g\text{-C}_3\text{N}_4$ were further confirmed by EDX data. EDX results of sulfated $g\text{-C}_3\text{N}_4$ and Au loaded sulfated $g\text{-C}_3\text{N}_4$ confirmed the presence of the expected elements (C, N, O, S and Au). EDX results of sulfated $g\text{-C}_3\text{N}_4$ shows the presence of sulfur in the samples. But after Au loading as some amount of sulfur leached out, EDX results of the Au loaded sulfated $g\text{-C}_3\text{N}_4$ shows very small amount of sulfur in the samples which is also confirmed by XPS data.

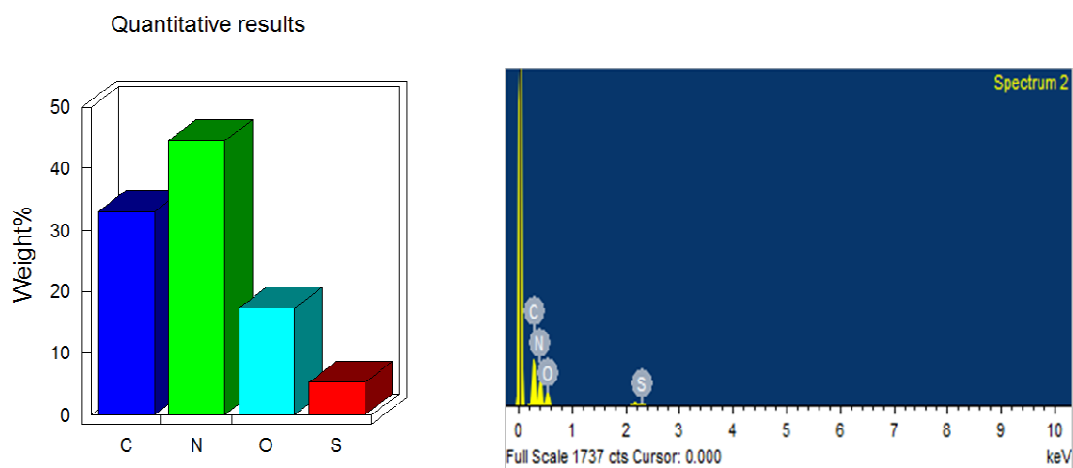


Figure 3 (a) EDX results of 9wt% sulfated $g\text{-C}_3\text{N}_4$

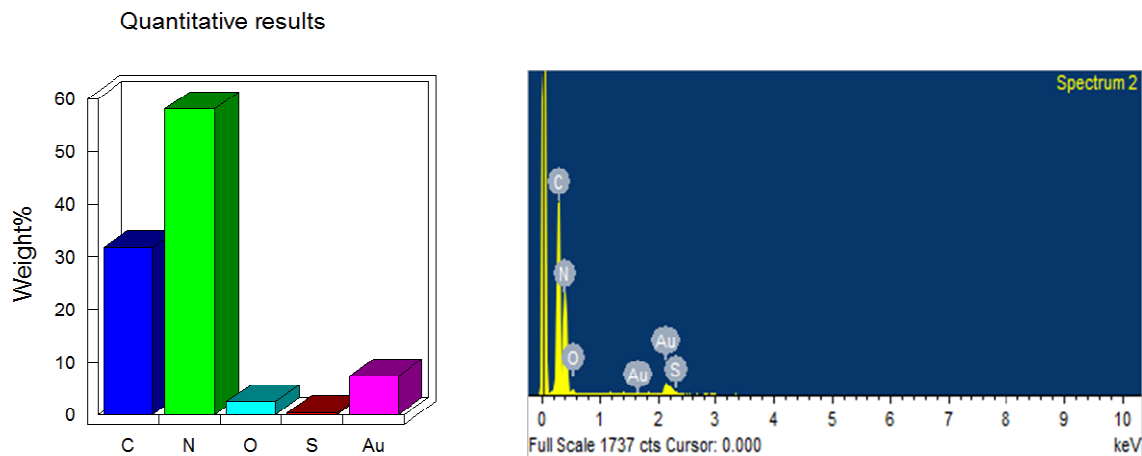


Figure 3 (b) EDX results of 1%Au-9wt% sulfated $g\text{-C}_3\text{N}_4$

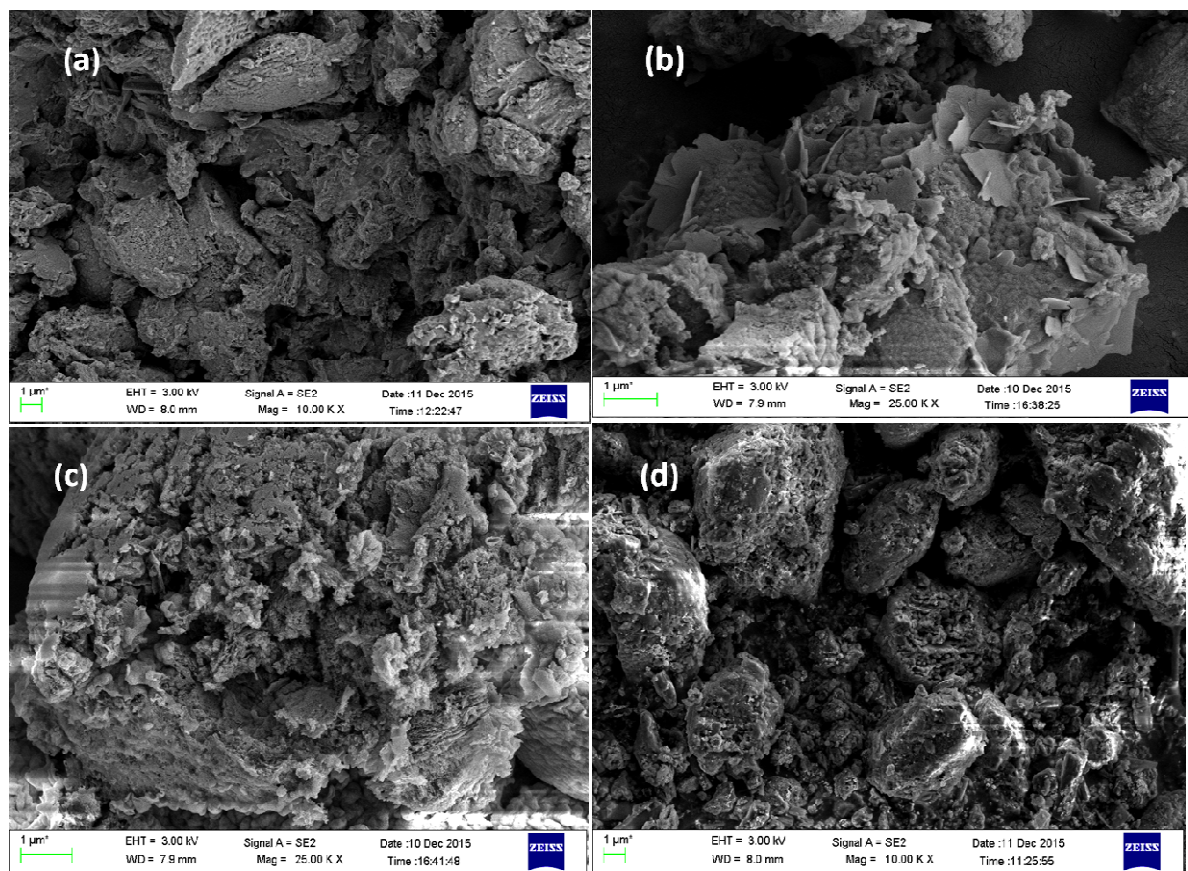


Figure 3 (c) SEM images of (a) neat $g\text{-C}_3\text{N}_4$ (b) and (c) 9% SO_4 $g\text{-C}_3\text{N}_4$ (d) 1%Au-9% SO_4 $g\text{-C}_3\text{N}_4$

TEM Study

The morphologies and microstructures of $g\text{-C}_3\text{N}_4$, 9% SO_4 $g\text{-C}_3\text{N}_4$ and Au-sulfated $g\text{-C}_3\text{N}_4$ nanocomposites were further investigated by transmission electron microscopy (TEM) in order to assess the crystalline behaviour, shape, size and pattern of distribution of Au NPs on the surface of $g\text{-C}_3\text{N}_4$. The TEM of neat $g\text{-C}_3\text{N}_4$ and 9% SO_4 $g\text{-C}_3\text{N}_4$ shows the layered structure of $g\text{-C}_3\text{N}_4$ (figure 4 (a) and (b)). From the TEM micrograph of 1%Au- $g\text{-C}_3\text{N}_4$ (Figure 4(c)), the uniform distribution of Au nanoparticles over the layered structure of C_3N_4 is clearly observed. Moreover, the distribution of Au nanoparticles increases significantly in case of sulphated $g\text{-C}_3\text{N}_4$ (Figure 4(d)) than that of neat $g\text{-C}_3\text{N}_4$. From the figure, it is confirmed that a direct physical assembly approach and perfect combination of sulfated $g\text{-C}_3\text{N}_4$ and Au NPs through electrostatic bonding, which is also in good agreement with the SEM observation. Moreover, the Au NPs are uniformly distributed on the entire surface of the $g\text{-C}_3\text{N}_4$ and also attached to the edges of $g\text{-C}_3\text{N}_4$ which acts as efficient visible-light absorber. The particles with dark colour can be assigned to Au NPs, whereas the grey area represents to $g\text{-C}_3\text{N}_4$. It is observed that $g\text{-C}_3\text{N}_4$ layers are well separated with no agglomeration. This confirmed presence of a strong interaction between $g\text{-C}_3\text{N}_4$ and Au NPs at the interface and resulted in the formation of Au/sulfated $g\text{-C}_3\text{N}_4$ composite photocatalyst, where the $g\text{-C}_3\text{N}_4$ sheet serve as a support and $-\text{HSO}_3$ groups as surfactant to bind with Au nanoparticles in the resulting composite system [9,14]. Moreover, the interfacial interaction favours electron migration process from the surface of $g\text{-C}_3\text{N}_4$ to Au NPs. From the TEM images it is revealed that, most of the Au NPs are dispersed in the range of 4-5 nm on $g\text{-C}_3\text{N}_4$ surface. The crystalline behaviour of Au NPs can be calculated from average fringe distance 2.36 Å which corresponds to 111 plane of Au and in consistent with other reported data.

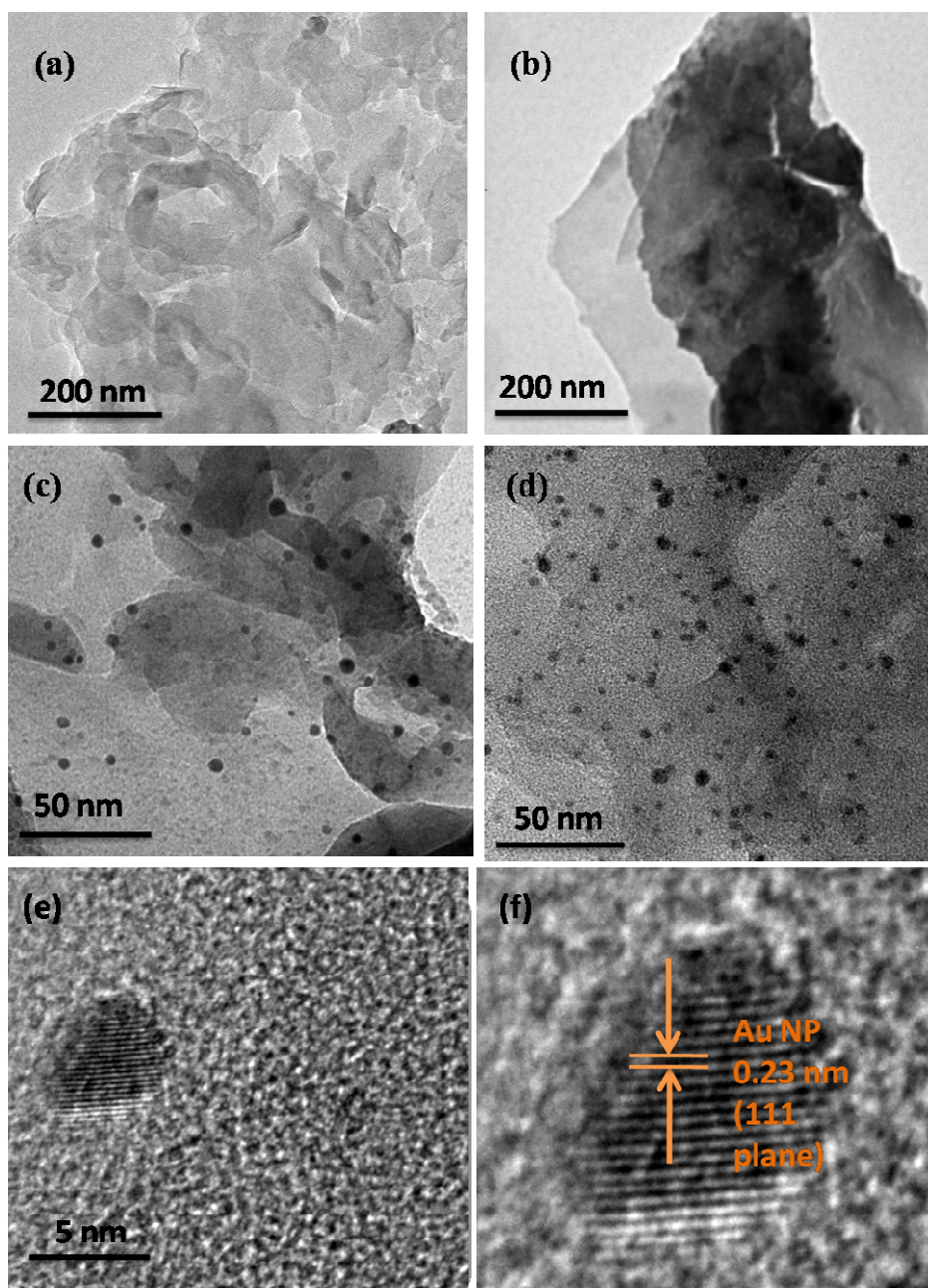


Figure 4 TEM images of (a) neat g-C₃N₄ (b) 9% SO₄ g-C₃N₄ (c) 1% Au-g-C₃N₄ (d) 1% Au-9% SO₄ g-C₃N₄ (e)&(f) shows the lattice fringes of Au

UV-Vis DRS analysis

The optical properties, effect of modification on the electronic structure, absorption edges and corresponding band gap energy of the prepared photocatalysts were analyzed by UV-Vis

diffuse reflectance spectroscopy and the results are shown in Figure 5(a) & (b). The absorption edge of neat g-C₃N₄ sample was estimated at approximately 450 nm and the calculated band gap energy was 2.77 eV. The optical absorption of the prepared plasmonic photocatalyst was found to cover the entire visible region of the solar spectrum. The optical absorption peaks after surface modification and Au loading were shifted remarkably to longer wavelength region and the corresponding band gap energy decreased to 2.48 eV and another at 1.5 eV due to plasmonic behaviour of Au NP [9] which promotes electron delocalization due to the extension of π -conjugated system. Red shift of absorption edge and the increased light absorption strongly indicates more visible light harvesting ability and narrowing of band gap energy producing photoinduced electrons and holes [20]. The anchoring of g-C₃N₄ sheets with -HSO₃ groups creates surface dyadic heterostructures which consequently effects the extension of electron channelization in the aromatic g-C₃N₄ sheets with modified structural connections and results bathochromic shift. The successful modification of the g-C₃N₄ matrix was also identified in naked eye by the change of colour from light yellow to greyish-brown after Gold loading. The enhanced absorbance intensities along with the enlarged surface areas are favourable to improve the photocatalytic performance significantly.

The band gaps of the synthesised samples were calculated by the Kubelka-Munk equation [7]

$$F(R) = K/S = (1-R)^2/2R$$

$$E_g = hv/\lambda = 1240/\lambda$$

where K represents the absorption coefficient, S represents the scattering coefficient, R represents the reflectance at the front face. F(R) is the Kubelka-Munk function and is an indicator of light absorption ability, with higher F(R) values representing stronger photoabsorption capacity. E_g the band gap Energy, and λ is the lower wavelength cut off region.

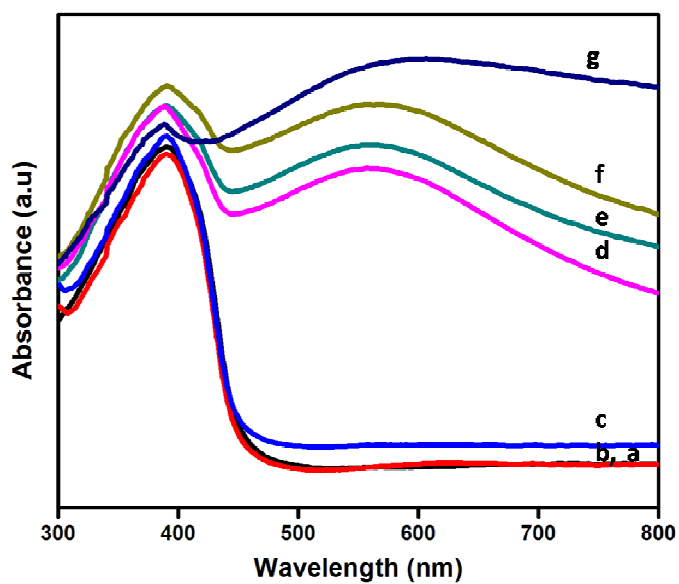


Figure 5 (a) Optical absorbance spectra of (a) neat g-C₃N₄ (b) 9% SO₄ g-C₃N₄ (c) 12% SO₄ g-C₃N₄ and (d) 1% Au-3% SO₄ g-C₃N₄ (e) 1%Au-6% SO₄ g-C₃N₄ (f) 1%Au-9%SO₄ g-C₃N₄ and (g) 1%Au-12% SO₄ g-C₃N₄

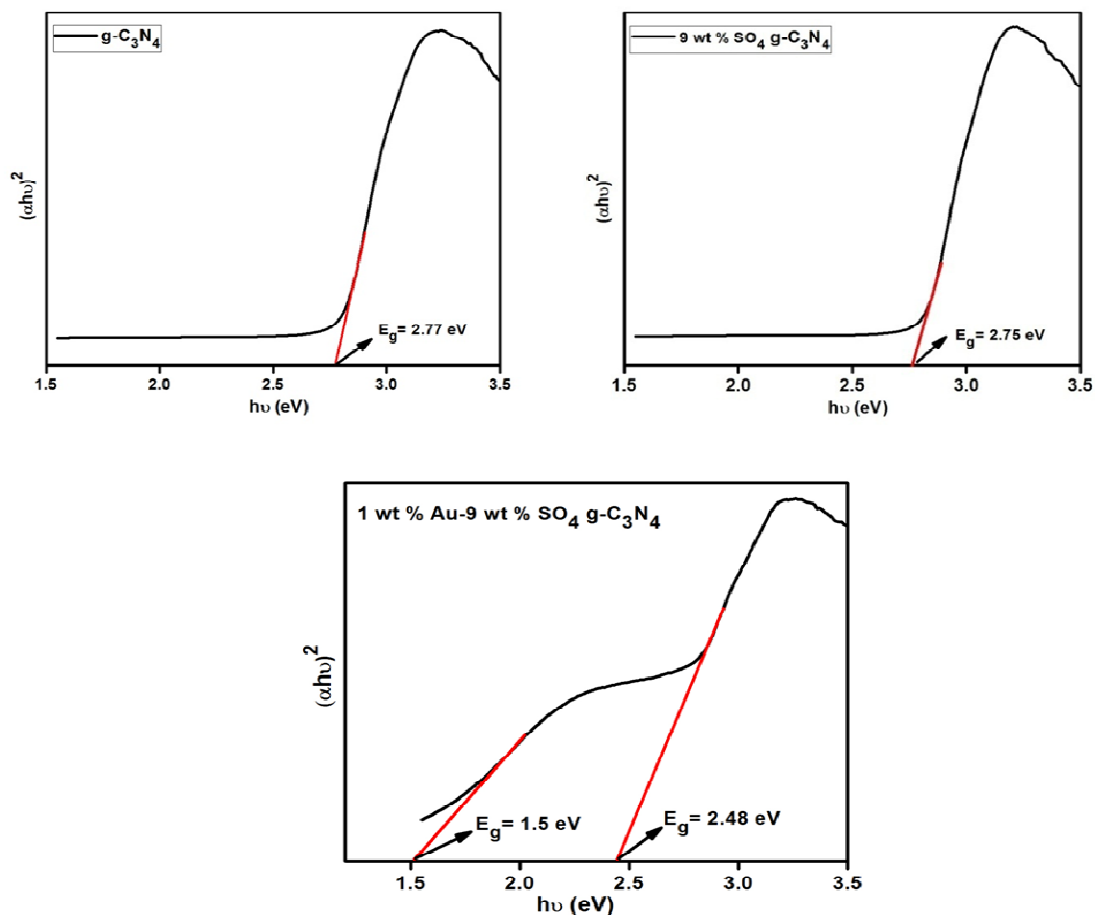


Figure 5 (b) Estimated band gap energies of neat $g\text{-C}_3\text{N}_4$, 9% SO_4 $g\text{-C}_3\text{N}_4$ and 1% Au-9% SO_4 $g\text{-C}_3\text{N}_4$ respectively

PL spectral analysis

Photoluminescence (PL) spectral analysis is used to reveal the structure-induced property change of the photocatalytic system. The PL emission spectra mainly give an idea about generation, migration and separation efficiency of photogenerated charge carriers in case of semiconductor photocatalysts. PL emission spectra of all the prepared samples, neat $g\text{-C}_3\text{N}_4$, sulfated $g\text{-C}_3\text{N}_4$ and AuNPs loaded sulfated $g\text{-C}_3\text{N}_4$ excited by 350 nm at room temperature shows emission peak of the neat $g\text{-C}_3\text{N}_4$ at 440 nm, which may be due to band–band recombination of the photogenerated electrons and holes with emission peak corresponding to its band gap energy. There is a significant decrease in the PL intensity in case of the sulfated $g\text{-C}_3\text{N}_4$, compared to that of the neat $g\text{-C}_3\text{N}_4$ as shown in figure 6 [21].

This significant decrease in the PL intensity obviously caused by the tunable narrowing of band gap and electron delocalization on the surface terminal sites of $g\text{-C}_3\text{N}_4$ due to the presence of $-\text{HSO}_3$ groups. However, there is a strong photoluminescence quenching with Au loading [9]. The significant fluorescence quenching in case of Au modified sample suggests an improved efficiency of photoexcited electron-hole separation. Among all nanocomposites, 1%Au-9% SO_4 $g\text{-C}_3\text{N}_4$ photocatalysts showed lowest PL intensity which suggests that the recombination of electron-hole pairs are effectively suppressed. Mostly poly-crystalline and nano-crystalline materials behave as radiative centres and as radiative traps during luminescence processes. As the Fermi level of the gold exists between the CB maximum and VB minimum of polymeric semiconducting material $g\text{-C}_3\text{N}_4$, the photo-excited electrons get transferred readily from the conduction band of $g\text{-C}_3\text{N}_4$ to the Au nano-particles. It indicates that in the nanocomposite photocatalysts more number of excited electrons are trapped and easily transferred through the interface due to the presence of Au nano-particles. The greatly prolonged lifetime of the charge carriers revealed that loading AuNPs on the surface of $g\text{-C}_3\text{N}_4$ improves the probability of their migration from the bulk to the interface, inhibits the recombination the charge carriers and thus facilitates the heterogeneous photocatalytic activity.

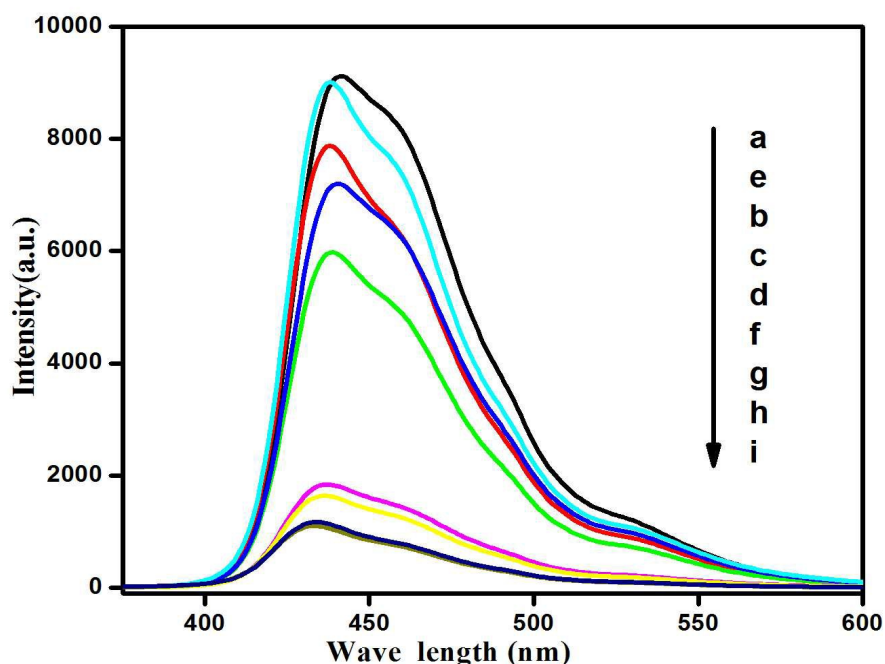


Figure 6(a) PL spectra of (a) neat g-C₃N₄, (b) 3%SO₄ g-C₃N₄ (c) 6%SO₄ g-C₃N₄ (d) 9%SO₄ g-C₃N₄ (e) 12%SO₄g-C₃N₄ (f) 1%Au-3%SO₄g-C₃N₄ (g)1%Au-6%SO₄ g-C₃N₄ (h)1%Au-12% SO₄ g-C₃N₄ (i) 1%Au-9%SO₄ g-C₃N₄ nanocomposite photocatalysts

Time-resolved photoluminescence

To gain more insight into the underlying of charge recombination and transfer process between the Au and sulfated g-C₃N₄, we have performed time-resolved PL experiments by taking the bulk g-C₃N₄, sulfated g-C₃N₄ and Au-loaded sulfated g-C₃N₄. Figure 6(b) shows the time-resolved PL spectra of bulk g-C₃N₄, sulfated g-C₃N₄ and Au-loaded sulfated g-C₃N₄ samples. To determine the life times of the charge carriers, the resulting PL decay emission plots are well fitted with the triexponential functions by the using eq. 1.

$$\text{Fit} = A_1.\exp(-t/T_1) + A_2.\exp(-t/T_2) + A_3.\exp(-t/T_3) \quad (1)$$

It is observed that the curves are best fit with the tri-exponential function. The decay components (τ_1 , τ_2 and τ_3) and the relative amplitudes of the decay species (A_1 , A_2 , A_3) are presented in Table-1.

The average lifetime of the materials were calculated to compare between the emission decay behavior of all the materials and to know the life time of the excited charge carriers. The average lifetime τ was calculated using the equation below [38]:

$$t(\text{av}) = \frac{A_1\tau_1^2 + A_2\tau_2^2 + A_3\tau_3^2}{A_1\tau_1 + A_2\tau_2 + A_3\tau_3} \quad (2)$$

It was clearly observed from the calculated data (Table 1) that the average life time of the excited charge carriers in case of 1%Au-9%SO₄g-C₃N₄ is 7.02 ns where as g-C₃N₄ and 9%SO₄ g-C₃N₄ exhibits 3.66 ns and 4.39 ns respectively. So the life time of the excited charge carriers is highest in case of 1% Au loaded 9%SO₄ g-C₃N₄. The longer life time of the charge carriers in case of 1% Au loaded 9%SO₄ g-C₃N₄ is mostly due to the loading of Au in sulfated g-C₃N₄. The data obtained from TRPL is also in agreement with PL spectra of the samples. The Fermi level of the gold exists in between the CB maximum and VB minimum of g-C₃N₄, the photo-excited electrons get transferred readily from the conduction band of g-C₃N₄ to the Au nano-particles. So more number of excited electrons are trapped and easily

transferred through the interface due to the presence of Au nano-particles in the nanocomposite photocatalysts. The longer lifetime of the charge carriers revealed that loading AuNPs on the surface of $g\text{-C}_3\text{N}_4$ improves the probability of their migration from the bulk to the interface, inhibits the recombination of charge carriers and thus facilitates the heterogeneous photocatalytic activity.

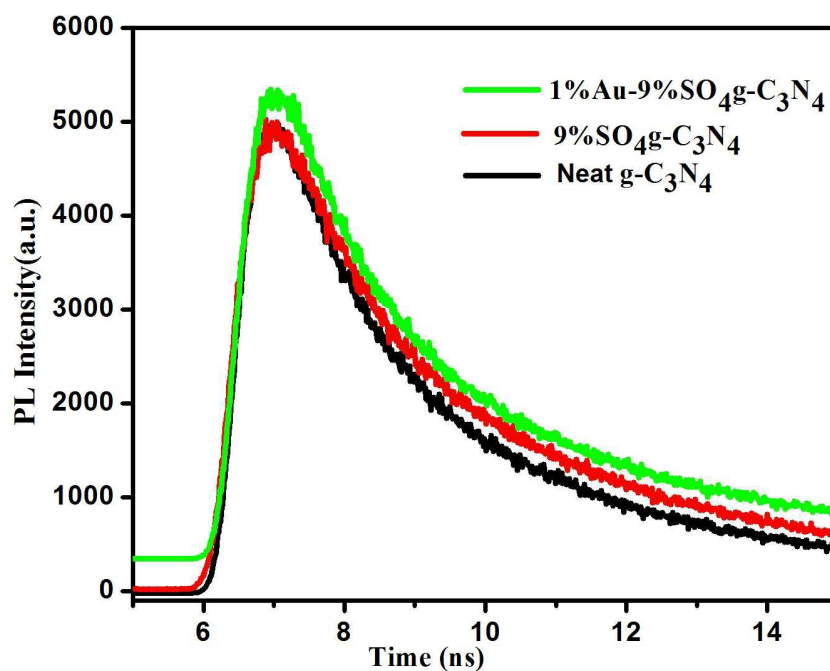


Figure 6 (b) TRPL spectra of (a) neat $g\text{-C}_3\text{N}_4$, (b) Sulfated $g\text{-C}_3\text{N}_4$ and (c) 1%Au-9%SO₄ $g\text{-C}_3\text{N}_4$ nanocomposite photocatalysts

Table 1 Summary of Average lifetime of charge carriers

Sample	$\tau_1(\text{ns})(A_1\%)$	$\tau_2(\text{ns})(A_2\%)$	$\tau_3(\text{ns})(A_3\%)$	$t_{\text{av}}(\text{ns})$
Neat- $g\text{-C}_3\text{N}_4$	0.727 (65)	2.9 (32)	10.4(3)	3.66
9%SO ₄ $g\text{-C}_3\text{N}_4$	0.4(51.6)	2.4(38.8)	7.9(9.6)	4.384
1%Au-9%SO ₄ $g\text{-C}_3\text{N}_4$	0.9(50)	3.9(41.66)	13.8(8.33)	7.023

X-ray photoelectron spectroscopy (XPS)

XPS is a surface-specific investigation technique, which can be used to determine the surface chemical compositions and formal oxidation state of all the elements present in the composite as shown in figure 7. Therefore, XPS measurements were performed to explicate the valence states of various elements (C, N, O, S and Au) present in the g-C₃N₄ and 1% Au 9% SO₄ g-C₃N₄. Fig. 7 shows the high-resolution XPS spectra of C 1s after Gaussian curve fitting. The C1s spectra can be deconvoluted into two peaks, representing two different oxidation states of carbon [22]. The peak observed at 284.9 eV corresponds to the sp²-hybridized carbon atom bonded to nitrogen atom present in the aromatic ring and the peak at 287.9.3 eV corresponds to the carbon atom bonded to three nitrogen atoms representing the same type of bonding states of C atoms in g-C₃N₄ structure as that of C atoms in melamine molecules.

The observed broad peak in figure 7 for N 1s has been resolved into three peaks at 397.3 eV, 398 eV, and 400 eV correspond to three different states of nitrogen [23,24]. The major peak observed at 397.3 eV was assigned to sp² hybridised nitrogen where the N-atom was bonded to two carbon atoms in two different ways (C=N-C). Another two peaks at 398 eV and 400 eV can be ascribed to tertiary N-atoms bonded to three carbon atoms (N-(C)₃) and one H-atom as N-H bonding. Those results confirm that there is no change in the electronic structures of C or N with the addition of Au.

The XPS spectra for O 1s in Fig.7 shows two different peaks centred at 531.5 and at 533 eV. The peak centered at 531 eV was attributed to -OH groups attached to the surface of g-C₃N₄ and the peak at 533 eV was due to the presence of surface -SO₃H groups [25]. A distinct peak at 168.5 eV should represent the oxidation state of S as S⁶⁺ [14]. But due to low percentage of sulfate, the sulfate peaks are not prominent, which confirms that during the reduction of Au³⁺ to metallic Au⁰, some amount of sulfate are leached out. In the synthesis procedure of Au loaded sulfated g-C₃N₄, after deposition of AuNPs the composite material was washed several times with hot water. During washing process sulphur is removed from the matrix. [35] Figure 7 shows only noisy peaks obtained for S 2p.

The two peaks centred at 83.37 eV and 87.0 eV originated from Au4f_{5/2} and 4f_{7/2} electrons of metallic gold explains the formation of Au⁰ [26]. Thus it confirms that the deposition-precipitation method effectively loaded nanosized particles of Au on the surface of the sulfated-g-C₃N₄, which is also in agreement with PXRD and HRTEM studies.

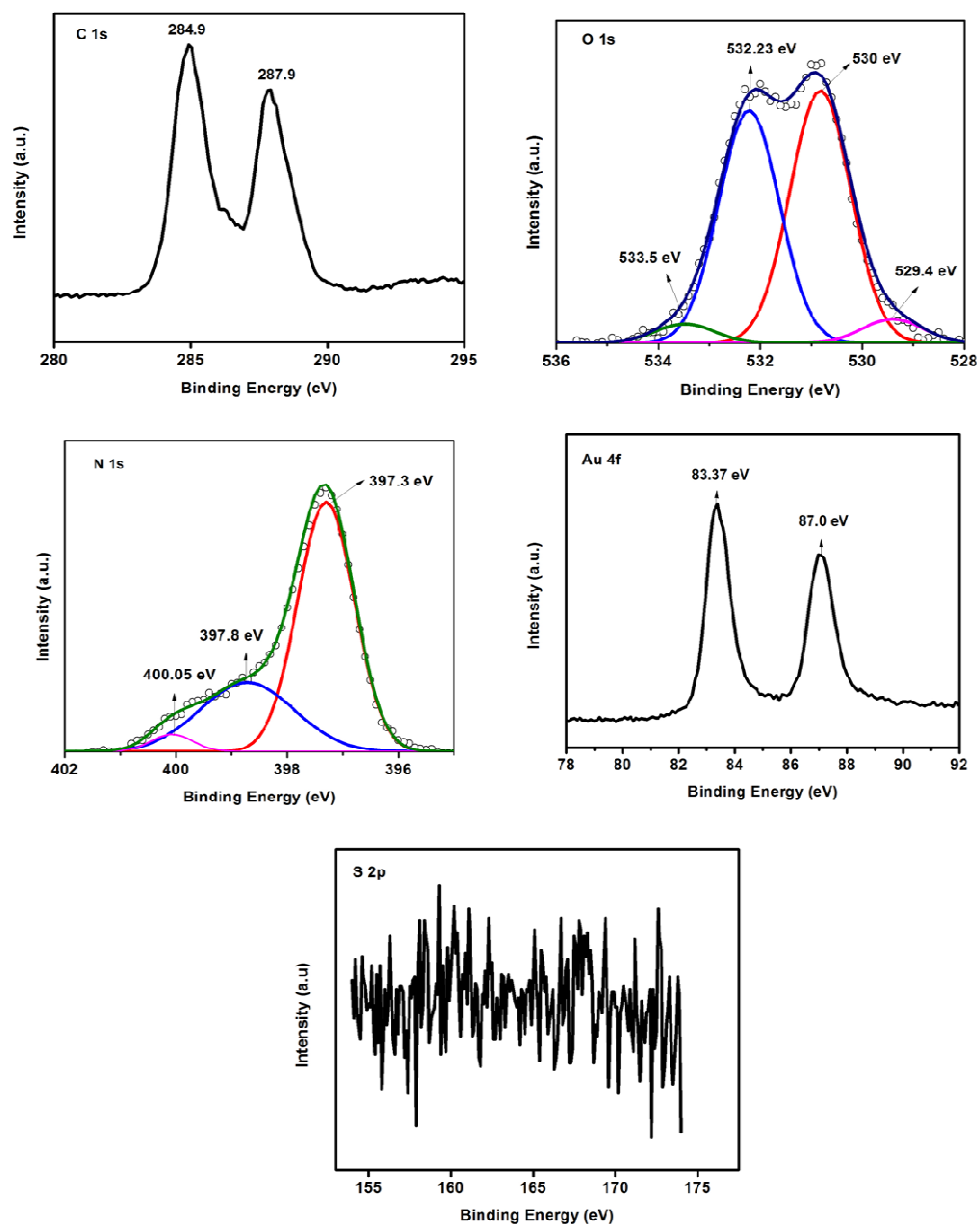


Figure 7 XPS spectra of C1s, O1s, N1s, Au4f and S2p in 1%Au-9%SO₄ g-C₃N₄

Photocatalytic hydrogen evolution

The photocatalytic activity of neat g-C₃N₄, sulfated g-C₃N₄ and all the AuNPs-incorporated sulfated g-C₃N₄ composites for H₂ evolution under visible light ($\lambda \geq 400$ nm) was measured by using a 10 vol% triethanolamine solution as a sacrificial hole scavenger and taking 0.02 g of powdered photocatalyst. A blank experiment was carried out under the same ambient

condition to confirm H_2 gas evolution, without using the photocatalyst. No hydrogen gas was found to evolve. After the addition of the prepared photocatalyst to the same sacrificial agent the evolution of hydrogen gas was found increased. Figure 8 (a, b) represents the photocatalytic hydrogen evolution rates of various nanocomposites. The average hydrogen evolution rate of sulfated $g-C_3N_4$ was much higher than that of neat $g-C_3N_4$ ($22 \mu\text{ mol h}^{-1}$) and after Au loading the hydrogen production was even higher than that reported for sulfated $g-C_3N_4$ and neat $g-C_3N_4$. The comparative data for hydrogen evolution over neat $g-C_3N_4$, 9% SO_4 $g-C_3N_4$, 1% Au $g-C_3N_4$ and 1%Au 9% SO_4 $g-C_3N_4$ nanocomposites is presented in Figure 8(C). Here in, the hydrogen production rate of 1wt% Au loaded sulphated $g-C_3N_4$ was found to be dramatically increased in comparison to neat $g-C_3N_4$. The photo catalytic H_2 evolution of the prepared composites are found to be a function of crystallinity of both $g-C_3N_4$ and Au nanoparticles. In this study, the H_2 evolution rate shows an increasing trend with sulphate treatment. However H_2 evolution decreases in case 1% Au-3% SO_4 - $g-C_3N_4$ and 1% Au-12% SO_4 - $g-C_3N_4$ because the crystallinity of both $g-C_3N_4$ and Au NPs are significantly less, as observed from XRD pattern.

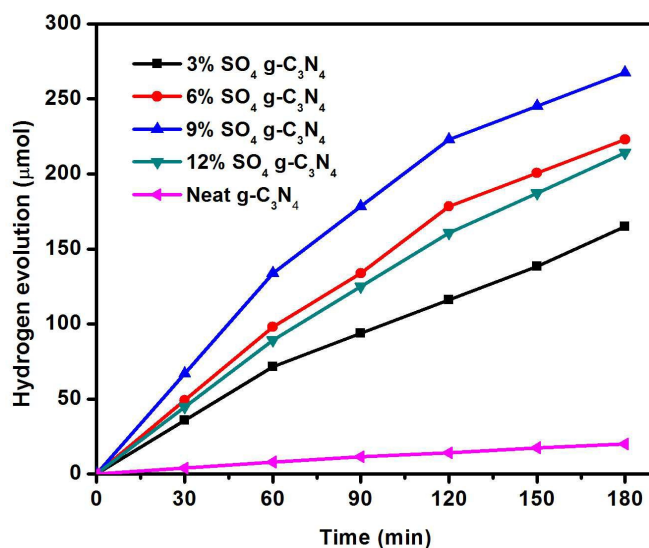


Figure 8 (a) Photocatalytic hydrogen evolution of neat $g-C_3N_4$, 3% SO_4 $g-C_3N_4$, 6% SO_4 $g-C_3N_4$, 9% SO_4 $g-C_3N_4$ and 12% SO_4 $g-C_3N_4$ nanocomposites under visible-light irradiation ($\lambda \geq 400$ nm)

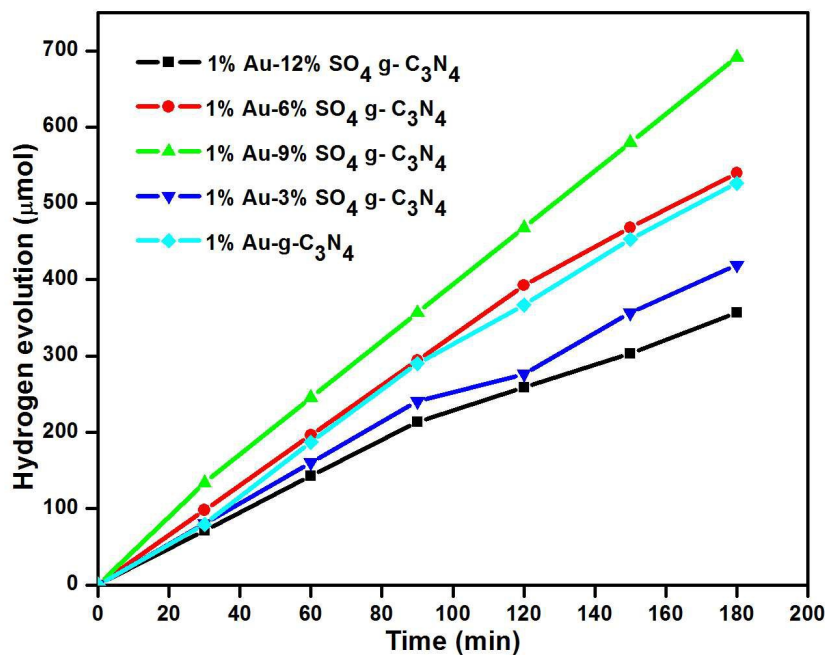


Figure 8 (b) Photocatalytic hydrogen evolution of 1% Au-g- C_3N_4 , 1% Au-3% SO_4 g- C_3N_4 , 1% Au-6% SO_4 g- C_3N_4 , 1% Au-9% SO_4 g- C_3N_4 and 1% Au-12% SO_4 g- C_3N_4 nanocomposites under visible-light irradiation ($\lambda \geq 400$ nm)

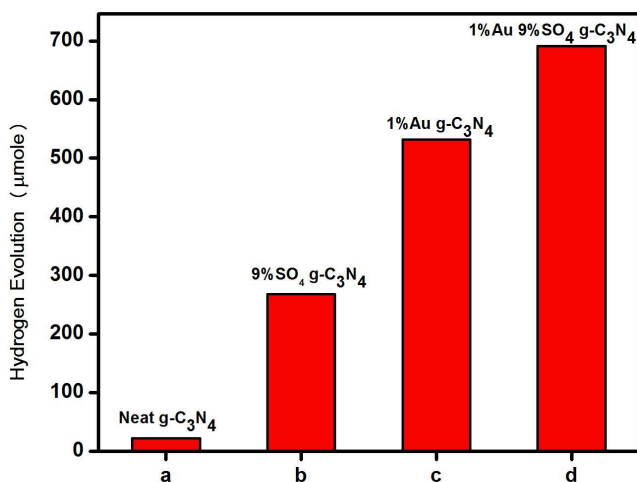


Figure 8 (c) A Comparative data of hydrogen evolution of neat g- C_3N_4 , 9% SO_4 g- C_3N_4 , 1% Au g- C_3N_4 and 1% Au 9% SO_4 g- C_3N_4 nanocomposites under visible-light irradiation ($\lambda \geq 400$ nm)

Both Au and sulphate synergistically combines to fulfil all the fundamental requirements of photocatalytic water splitting through their electronic environment and found to be a promising photocatalyst towards water splitting. To confirm the stability of the catalyst, recyclability test was done by evacuating reactor by purging N₂ gas. The experiment was performed for four cycles with an induction period of 3 h. In each cycle the same activity was found which confirms the stability of the photocatalyst as shown in figure 8(d).

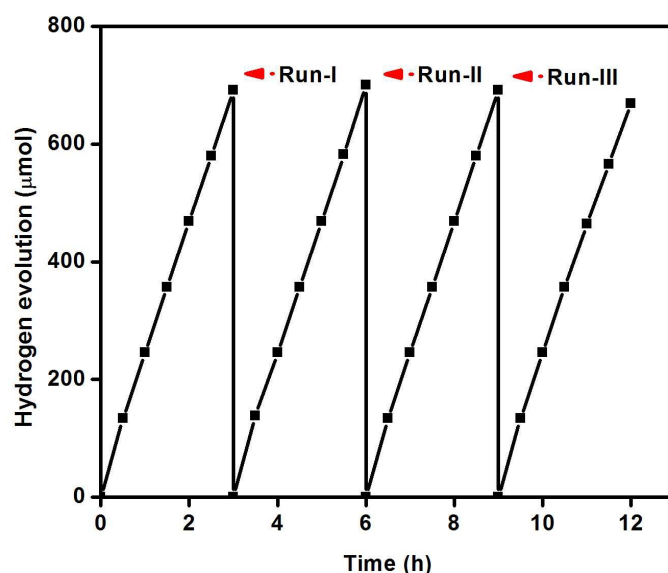


Figure 8 (d) Reusability study of 1% Au-9% SO₄ g-C₃N₄ for Photocatalytic H₂ evolution under visible-light irradiation ($\lambda \geq 400$ nm)

Explanation for increased photocatalytic activity

The increased photocatalytic ability of Au loaded sulfated g-C₃N₄ nanocomposites, may be attributed to

1. The synergistic effect of sulfonic group and Au nano-particles
2. Presence of p-phenyl-SO₃H groups on the surface as well as the edge of g-C₃N₄ sheet although to a small extent improves the functionality of the material.
3. Upon protonation in the process of sulfate pretreatment defects are introduced into g-C₃N₄. Owing to which Sulfonated g-C₃N₄ possesses adequate number of surface

active sites to make AuNPs to adhere g-C₃N₄ plane firmly because of defected surface by creating oxygen vacancies. It can be said that this favours the adsorption of AuNPs onto the created vacant oxygen sites [8]. AuNPs preferably get adsorb on these reduced surfaces and increases the extent of the electron channelization between gold and the g-C₃N₄ interface. This sulfonation not only influence homogeneous distribution of AuNPs by forming superior electronic junction but also improves the efficiency of sulfate treated samples compared to non-sulfated ones.

4. Presence of electrostatic attraction between sulphur and AuNPs favours to improve crystallinity .
5. Shifting of the Fermi level Au towards more negative potential due to localized surface plasmon resonance (LSPR).
6. Increasing capability of light absorption of AuNP loaded sulfate pre-treatment g-C₃N₄ nanocomposites due to significant reduction in band gap energy.
7. The high separation efficiency and channelization of the photo-generated charge carriers, due to the presence of highly mobile excitons in the central portion of the functionalised g-C₃N₄ sheet, and leaving more photogenerated electrons to remain on the surface for reaction.

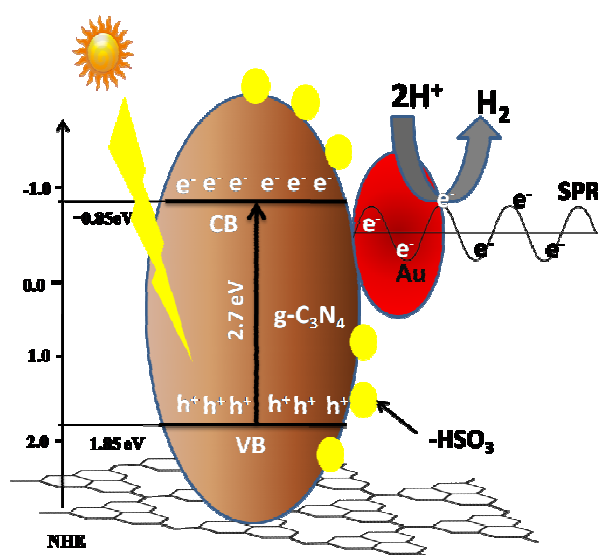
In case of a layered material, the existence of Vander Waals forces makes the layered material (g-C₃N₄) prone to aggregation [27,28], which hinders the deposition of NPs on its surface. Hence the purpose of sulfonation is to enhance the surface functionality by introducing -SO₃H groups. Sulfated g-C₃N₄ not only increases the surface functionality but also generates a defected surface by creating oxygen vacancies [8]. Owing to the presence of electronegative sulphur, positively charged Au particles get preferably attracted to the sulphur atom due to electrostatic attraction and in turn get reduced. The XRD image reveals clear information about the enhanced crystallinity of Au NPs due to the presence of sulfur atom in g-C₃N₄ sheet. Although the wt% of Au in all the samples were the same but the peak intensity of Au increases with increase in sulfate amount in sulfate pre-treatment g-C₃N₄ samples. It is observed that the improved photocatalytic performance of a material is associated with higher crystallinity and fewer bulk defects. Hence, sulfated g-C₃N₄ shows great potential to adhere AuNPs because of enhanced functionality of g-C₃N₄. The presence of porosity and interconnectivity morphology between the AuNPs and g-C₃N₄ through sulfate treatment improves the charge separation efficiency and suppresses the charge carrier recombination.

Sulphated $g\text{-C}_3\text{N}_4$ increases the surface functionality and develops porosity in the material. Owing to that sulfated $g\text{-C}_3\text{N}_4$ photocatalyst exhibits an enhanced specific surface area of $16.3 \text{ m}^2/\text{g}$. However, AuNPs deposited sulfated $g\text{-C}_3\text{N}_4$ photocatalyst showed slight increase in specific surface area to $19.1 \text{ m}^2/\text{g}$. The functionalized $-\text{SO}_3\text{H}$ groups act as the bridge to deposit AuNPs on the surface of $g\text{-C}_3\text{N}_4$. Although the transport of the photo-generated charge carriers from the surface of the $g\text{-C}_3\text{N}_4$ to the AuNPs is delayed due to indirect contact between AuNPs and $g\text{-C}_3\text{N}_4$, but the excited photo electrons can easily move through the sulfated $g\text{-C}_3\text{N}_4$ sheet through $\pi\text{-}\pi$ conjugation, thus efficiently reduce the probability of recombination. Colloids of noble metals such as Ag, Au, Pt are found to be air-stable and their plasma frequency lies in the visible region of the solar spectrum owing to d-d band transition and they behave as surface plasmons. The resonance frequency of surface plasmon is strongly dependent on the particle dimension of noble-metal nanoparticles, its shape, inter-particle interactions, dielectric properties and the environment of the nanoparticles [28-30]. The oscillation frequency of noble metal nanoparticles is critically governed by four factors: the density of electron cloud, the effective electron mass, the shape and the dimension of charge distribution. The role of Au NPs are found to be superior among all noble metals for photocatalytic hydrogen production owing to their surface Plasmon effects, low photoluminescence intensity, reduced band gap energy, excellent visible light absorption[31-33]. Taking into account the importance of loading AuNPs, it is found that after loading of Au NPs on sulfated $g\text{-C}_3\text{N}_4$ sheet the photocatalytic performances of $g\text{-C}_3\text{N}_4$ was further improved. Similar observation was made by our group in case of Au promoted sulphated metal oxides [34]. This increased activity due to AuNPs was also supported by other reported facts of our group. Pany et al. studied Au modified sulfated metal oxide by varying the wt % of gold where the enhanced activity was due to synergetic effect of Au and sulphate as redox couple [35]. Our group has also studied extensively the effect of sulphate treatment on the photocatalytic activity of metal oxides [36]. In another study also we have reported role of nano-Au in enhancing the activity of S,N doped mesoporous metal oxide nanocomposite [36].

When the surface of polar $g\text{-C}_3\text{N}_4$ is irradiated with visible light of the solar spectrum, electrons get excited from the VB to the CB and holes are left in the valence band. In turn a Mott-Schottky junction was formed at the interface of AuNPs and polar sulfated $g\text{-C}_3\text{N}_4$ [34,35]. Absorption of visible light radiation by AuNPs results in the coherent oscillation of the conduction band electrons inducing its interaction with the electromagnetic field. This type of coupled oscillation of electromagnetic field with the conduction band electrons of

AuNPs results in the formation of surface plasmons [35]. The opto-electronic properties of AuNPs were greatly dependent on these types of coupled oscillations. The deposited Au NPs on sulfated $g\text{-C}_3\text{N}_4$ surface were polarized and by its plasmonic effect scattered the visible light. As the Fermi level of the Au NPs exists between the conduction band maximum and valence band minimum of polar sulfated $g\text{-C}_3\text{N}_4$, the surface electronic wave can easily propagate at the interface between the $g\text{-C}_3\text{N}_4$ and AuNPs owing to the formation of plasmonic photocatalysts [36].

The conduction band potential of polar semiconducting $g\text{-C}_3\text{N}_4$ was more negative than the redox potential of standard H^+/H_2 , which was the most important requirement for evolution of hydrogen. The increased visible light absorption results accumulation of good number of electrons in the conduction band of $g\text{-C}_3\text{N}_4$. These excitons from the conduction band of $g\text{-C}_3\text{N}_4$ readily transferred to the Au NPs at the interface showing enhanced activity of the photo-catalyst by reducing the band gap energy. Moreover, the electron channelization from sp^2 -hybridized π -conjugated $g\text{-C}_3\text{N}_4$ network to Au surface through the $-\text{HSO}_3$ group shifts the Fermi level of AuNPs towards more negative potential. The delayed electron-hole recombination and accumulated electronic charge density on AuNPs more easily reduced water molecules to liberate hydrogen gas in presence of a suitable sacrificial hole scavenger which were partially oxidized by the holes, and hinders the process of electron-hole recombination.



Scheme 2 Mechanism of photocatalytic hydrogen production and surface plasmon resonance of AuNPs in Au/sulfated g-C₃N₄ nanocomposite.

Conclusions

In summary, deposition of gold nanoparticles over sulphated g-C₃N₄ seemed to be a gifted photocatalyst for hydrogen gas production. In our work, we have presented a novel strategy for the production of a structure-controlled gold loaded sulfated g-C₃N₄ in which sulfate was loaded by impregnation method and gold by borohydrate reduction method. The defected surface of sulfate pre-treated g-C₃N₄ strengthens the adsorption of AuNPs onto the vacant oxygen sites. XPS data confirmed the AuNPs get adsorbed on the reduced surfaces, increasing the extent and effectiveness of the electronic communication between gold and the g-C₃N₄ interface. The visible light induced water reduction for H₂ production of Au-sulfated g-C₃N₄ was increased over 2.5 times than that of sulfated g-C₃N₄, 1.5 times than that of Au-g-C₃N₄ and 35 times more than that of single phase g-C₃N₄. The enhancement in photocatalytic activity for hydrogen evolution of Au loaded sulfated g-C₃N₄ is in well agreement with efficient visible light absorption, SPR effect of Au nanoparticles, efficient adsorption of AuNPs by pre-sulfated g-C₃N₄ and low electron-hole recombination process. This interesting result of improved optical absorption for the sustainable utilization of solar radiation provides a feasible chemical pathway for constructing polymeric systems for the application in photocatalysis, PEC, life science, such as drug delivery or bioimaging.

References

1. S. Yang, G. Gong, J. Zhang, L. Zhan, L. Ma, Z. Fang, R. Vajtai, X. Wang and P.M. Ajayan, *Adv. Mater.* 2013, **25**, 2452–2456.
2. S. Patnaik, S. Martha and K.M. Parida, *RSC Adv.*, 2016,**6**, 46929-46951.
3. Z.Wang, W. Guan, Y. Sun, F. Dong, Y. Zhou and W.K. Ho, *Nanoscale*. 2015 ,**7**,2471–2479.
4. M. Li, L. Zhang, X. Fan, Y. Zhou, M. Wu and J. Shi, *J. Mater. Chem. A*, 2015, **3**, 5189–5196.
5. S. Nayak, L. Mohapatra and K.M. Parida, *J. Mater. Chem. A*, 2015, **3**(36),18622-35.
6. S. Patnaik, S. Martha, S. Acharya and K. M. Parida, *Inorg. Chem. Front*, 2016,**3**,3 336-347.

7. Y. Fan, D. Han, B. Cai, W. Ma, M. Javed, S. Gan, T. Wu, M. Siddiq, X. Dong and L. Niu, *J. Mater. Chem. A*, 2014, **2**, 13565–13570.
8. M.C. Hidalgo, M. Maicu, J.A. Navío and G. Colón, *J. Phys. Chem. C*, 2009, **113**, 12840–12847.
9. S. Samanta, S. Martha and K. Parida, *ChemCatChem*, 2014, **6**, 1453-1462.
10. Y. Zhang, A. Thomas, M. Antonietti and X. Wang, *J. Amer. Chem. Soc.*, 2009, **131**, 50–51.
11. T. Y. Ma, Y. Tang, S. Dai and S. Z. Qiao, *small*, 2014, **10**, 2382–2389
12. H. Yan, Y. Chen and S. Xu, *Int J Hydrogen Energy*, 2012, **37**, 125-133
13. F. Cheng, H. Wang and X. Dong, *Chem. Commun.*, 2015, **51**, 7176-7179.
14. S. Chang, A. Xie, S. Chen and J. Xiang, *J. Electroanal. Chem.*, 2014, **719**, 86–91
15. J. A. Singh, S. H. Overbury, N. J. Dudney, M. Li and G. M. Veith, *ACS Catal.* 2012, **2**, 1138–1146
16. N. Cheng, J. Tian, Q. Liu, C. Ge, A. H. Qusti, A. M. Asiri, A. O. Al-Youbi and X. Sun, *ACS Appl. Mater. Interfaces*, 2013, **5**, 6815–6819.
17. J. Xue, S. Ma, Y. Zhou, Z. Zhang and M. He, *ACS Appl Mater Interfaces*, 2015, **18**, 9630-9637.
18. S. Martha, A. Nashima and K.M. Parida, *J. Mater. Chem. A*, 2013, **1**, 7816–7824.
19. Z. Wang, W. Guan, Y. Sun, F. Dong, Y. Zhou and W.K. Ho, *Nanoscale*. 2015, **7**, 2471–2479.
20. J.H. Liu, T.K. Zhang, Z.C. Wang, G. Dawson and W. Chen, *J. Mater. Chem.* 2011, **21**, 14398-14401.
21. S. Martha, K.H. Reddy, N. Biswal and K. Parida, *Dalton Trans.*, 2012, **41**, 14107–14116.
22. F. Dong, L.W. Wu, Y.J. Sun, M. Fu, Z.B. Wu and S.C. Lee, *J. Mater. Chem.* 2011, **21**, 15171-15174.
23. S. Pany and K.M. Parida, *Phys. Chem. Chem. Phys.*, 2015, **17**, 8070–8077.
24. P. Zhang, C.L. Shao, X.H. Li, M.Y. Zhang, X. Zhang, Y.Y. Sun and Y.C. Liu, *J. Hazard. Mater.* 2012, **237**, 331-338.
25. Y. Zhang, Z.R. Tang, X. Fu and Y.J. Xu, *ACS Nano*, 2010, **4**, 7303–7314.
26. G. Williams, B. Seger and P.V. Kamat, *ACS Nano*, 2008, **2**, 1487–1491.

27. M. Meier and A. Wokaun, *Opt. Lett.* 1983, **8**, 581-583.
 28. C.C. Lam, P.T. Leung and K. Young, *J. Opt. Soc. Am. B*, 1992, **9**, 158,
 29. C.J.G. Silva, Ju_rez, R.T. Marino, R. Molinari and H. Garc, *J. Am. Chem. Soc.* 2011, 133, 595– 602.
 30. L.A. Lyon, D.J. Pena and M.J. Natan, *J. Phys. Chem. B*, 1999, **103**, 5826–5831.
 31. S.Link and M.A. El-Sayed, *J. Phys. Chem. B*. 1999, **103**, 8410-8426.
 32. V. Subramanian, E.E. Wolf and P. Kamat. *J. Am. Chem. Soc.* 2004, **126**, 4943–4950.
 33. S.K. Ghosh and T. Pal, *Chem. Rev.* 2007, **107**, 4797 – 4862.
 34. M.V. Dozzi, L. Prati, P. Canton and E. Selli, , *Phys. Chem. Chem. Phys.*, 2009, **11**, 7171-7180.
 35. S. Pany, B. Naik, S. Martha and K. Parida, *ACS Appl. Mater. Interfaces*, 2014, **6**, 839–846.
 36. B.Naik, K.M. Parida and C.S. Gopinath, *J. Phys. Chem. C*, 2010, 114 ,19473–19482.
 37. K . M . Parida, N. Sahu, A.K. Tripathy and V. S. Kamble, *Environ. Sci. Technol.* 2010, **44**, 4155–4160.
 38. B. Choudhury and P. K. Giri, *RSC Adv.*, 2016, **6**, 24976-24984.
-